Critical issues in the CFD simulation of Darrieus wind turbines

Critical issues in the CFD simulation of Darrieus wind turbines

Francesco Balduzzi, Alessandro Bianchini, Riccardo Maleci, Giovanni Ferrara

Lorenzo Ferrari*

Francesco Balduzzi - Department of Industrial Engineering, University of Florence

Via di Santa Marta 3, 50139, Firenze, Italy

Tel.: +39 055 4796 570 - Fax: +39 055 4796 342 - E-mail: balduzzi@vega.de.unifi.it

Alessandro Bianchini - Department of Industrial Engineering, University of Florence

Via di Santa Marta 3, 50139, Firenze, Italy

Tel.: +39 055 4796 570 - Fax: +39 055 4796 342 - E-mail: bianchini@vega.de.unifi.it

Riccardo Maleci - Department of Industrial Engineering, University of Florence

Via di Santa Marta 3, 50139, Firenze, Italy

Tel.: +39 055 4796 570 - Fax: +39 055 4796 342 - E-mail: maleci@vega.de.unifi.it

Giovanni Ferrara - Department of Industrial Engineering, University of Florence

Via di Santa Marta 3, 50139, Firenze, Italy

Tel.: +39 055 4796 402 - Fax: +39 055 4796 342 - E-mail: giovanni.ferrara@unifi.it

Lorenzo Ferrari - CNR-ICCOM, National Research Council of Italy

Via Madonna del Piano 10, 50019, Sesto Fiorentino, Italy

Tel.: +39 055 5225 218 - Fax: +39 055 5225 203 - E-mail: lorenzo.ferrari@iccom.cnr.it

* = *corresponding author*

Abstract

Computational Fluid Dynamics is thought to provide in the near future an essential contribution to the development of vertical-axis wind turbines, helping this technology to rise towards a more mature industrial diffusion. The unsteady flow past rotating blades is, however, one of the most challenging applications for a numerical simulation and some critical issues have not been settled yet.

In this work, an extended analysis is presented which has been carried out with the final aim of identifying the most effective simulation settings to ensure a reliable fully-unsteady, two-dimensional simulation of an H-type Darrieus turbine.

Moving from an extended literature survey, the main analysis parameters have been selected and their influence has been analyzed together with the mutual influences between them; the benefits and drawbacks of the proposed approach are also discussed.

The selected settings were applied to simulate the geometry of a real rotor which was tested in the wind tunnel, obtaining notable agreement between numerical estimations and experimental data. Moreover, the proposed approach was further validated by means of two other sets of simulations, based on literature study-cases.

Keywords: *CFD, Darrieus, wind turbine, simulation, unsteady, sensitivity analysis*

1. Introduction

Darrieus Vertical-Axis Wind Turbines (VAWTs) are receiving increasing interest in the wind energy scenario, as this turbine typology is thought to represent the most suitable solution in non-conventional installation areas, due to the reduced variations of the power coefficient even in turbulent and unstructured flows (Refs. from [1] to [7]), with low noise emissions and high reliability. Moreover, this technology is also gaining popularity for large-size floating off-shore installations (e.g. [8]).

The design and development of these rotors have been historically carried out with relatively simple computational tools based on the BEM (Blade Element Momentum) theory [9]-[12]. This kind of approach can still provide some advantages in many cases, especially concerning the preliminary design of a machine (e.g. overall dimensions and attended power), as it is generally quite reliable and with very reduced computational cost [9]. In addition, some more advanced techniques are presently available like wake models, vortex models or the Actuator Cylinder flow model [13].

As discussed by several authors (e.g. [14]-[15]), however, an accurate modeling of these machines cannot disregard anymore the recent developments in CFD simulations, as they can significantly contribute to the technological improvement in designing the rotors, needed to rise the technology towards a well-established industrial production. On this basis, one can easily argue that the goal of assessing a reliable approach to CFD simulation of Darrieus turbines is thought to represent one of the most challenging prospects for the future wind energy research.

Some of the most complex and less understood phenomena in the field of numerical simulations are involved in the analysis of the flow past rotating blades [9]. With particular reference to Darrieus wind turbines, the problems to be solved to correctly describe the flow field developing around the turbine are increased by the constant variation of the incidence angle with the azimuthal position of the blade and the strong interaction between the upwind and the downwind halves of the rotor ([9] and [12]). Moreover, a major aspect of the unsteady aerodynamics of Darrieus rotors is represented by dynamic stall, which often occurs at low tip-speed ratios (TSRs), where the range of variation of the incidence angle on the airfoils is larger ([9] and [16]-[17]).

Within this scenario, a relevant aspect which has not been often discussed in sufficient detail in the technical literature is the "philosophical" approach to CFD simulations, i.e. the goal of the simulations themselves and the most suitable tools to achieve it. In detail, if one would go through the problem with a logical approach, two main observations can be promptly made:

- The functioning principle of vertical-axis wind turbines, where the flow conditions seen by the blades changes instant by instant as a function of the position occupied in the revolution trajectory, made any typology of simulation definitely ineffective, with the only exception of a fully unsteady approach (i.e. the only able to catch the real interactions between the blades).
- Based on the above, the circumferential symmetry cannot be exploited like in many other turbomachinery applications: the full revolution of the blade must hence be described, leading to very heavy simulations in terms of mesh size and computational time.

Moving forward in the analysis, although the three-dimensional approach is the only able to really describe the flow field around the turbine (i.e. also the real performance), some considerations are here proposed to focus the attention on benefits, drawbacks and requirements of the a 2D or a 3D approach. In particular:

- A 3D approach is needed in case the simulations are deemed to provide the attended power output of the rotor. In these cases, the influence of spanwise velocity components, tip effects and interactions with the "parasitic" components (e.g. struts, tower, etc.) cannot indeed be neglected ([9], [12] and [18]).

- By doing so, enormous computational resources are generally needed [19] and in some cases (e.g. [20]) authors have proposed to apply different settings to three-dimensional simulations with respect to what has been defined for the "lighter" two-dimensional calculations.
- Some applications, however, do not indeed require an exact estimation of the overall performance of the rotor. In particular, if properly assessed, a 2D approach could be successfully applied to the analysis of many relevant issues connected to the functioning of Darrieus rotors, like the dynamic stall, the flow curvature effects and the wake interaction with the downwind half of the revolution [9]. Moreover, a reliable 2D simulation, coupled with simplified models to account for the main secondary effects [12], could also provide a first estimation of the overall performance of the rotor, to be compared and integrated with the results of the BEM codes conventionally exploited by industrial manufacturers.

Based on the above and observing that no agreement was found between the most accredited literature sources, in this work an extended analysis on the critical issues to properly perform a 2D simulation of a Darrieus rotor is presented and discussed. The assessment of a reliable setting for this type of approach can provide a very useful tool to more in depth analyze the real functioning of the turbines; contemporarily, it could represent the basis for a future extension of the analysis to full 3D models.

2. Literature review

The ongoing evolution of CFD solvers is providing new opportunities for wind turbine designers to enhance the comprehension of the real blades-flow interaction; in addition, the diffusion of commercial codes is thought to guarantee in the next future reliable tools for the development of new machines, with noticeable cost and time savings. On the other hand, the great advantages of CFD simulations in such complex phenomena, like those connected to rotating blades, can be nullified if unsuitable settings are implemented by the user. In particular, a proper definition of the computational parameters can be obtained only by means of a thorough sensitivity analysis on the influence of these variables on the results accuracy, possibly coupled with a validation study based on experimental data.

Within the present study, a detailed review on the state-of-the-art of numerical approaches for the simulation of Darrieus turbines was first carried out by the authors. Upon examination of the literature, several works were identified ([15] and [20]-[39]), all published in the past five years; as one may then notice, the topic is still quite

new and there is a lack of extensive studies for the definition of practical guidelines to properly model the flow around a Darrieus turbine's blade.

As a result, even though the considered studies are all focused on the evaluation of the average power coefficient as a function of the TSR and/or the instantaneous power coefficient as a function of the azimuthal position of the blade, poor agreement was found on the most suitable settings to be adopted for the simulation. An effective convergence was indeed found only on the bases of the simulating approach, i.e.:

- The unsteady approach ([15] and [20]-[34]) is largely preferred to the steady-state ([35]-[37]) or to the multiple reference frame ([38] and [39]) approaches. In the unsteady approach, the rotating machine is simulated with two distinct sub-grids: a circular zone containing the turbine geometry, and rotating with its angular velocity, and a fixed outer zone (with a rectangular shape in most cases), which defines the boundaries of the overall calculation domain. The two regions communicate by means of a sliding interface.
- Boundary Conditions: as widely accepted for similar simulations, a velocity inlet and a pressure outlet are used in the mainstream direction, whereas lateral boundaries are threated either as solid walls or with the symmetry condition ([15], [20]-[22], [24], [27]-[28], [30], [33], [35]-[36]).
- A fully 3D approach is rarely adopted ([33], [34] and [38]). In all other cases, a 2D approach is basically used, sometimes compared with a 3D attempt with very raw settings due to the enormous calculation costs ([20]-[21], [23], [30] and [37]).
- The simulations are mainly performed with the commercial code ANSYS® Fluent® ([15], [21]-[24], [26]-[29], [31] and [33]-[36]).
- The accuracy of the numerical results is usually checked by means of experimental data derived from wind tunnel measurements ([15], [21]-[26], [28]-[29]).

Since the present study was conceived in view of a 2D unsteady approach, a more extensive analysis of the studies [15] and [20]-[32] is given in Table 1; the goal of this comparative analysis was in fact to highlight whether some general tendencies could have been found among the considered cases.

In particular, the benchmark was focused on the followings parameters:

- Turbulence modeling approach and models
- Numerical settings (solution algorithm and methods for the discretization of the N-S equations)
- Time-dependent solution settings (angular discretization and global duration of the calculation)
- Distance of the domain boundaries (inlet, outlet, lateral and sliding interface) from the turbine

- Discretization of the boundary layer (y^+ and number of nodes on the airfoil contour)
- Overall number of mesh elements and mesh typology

No agreement was found on the choice of the turbulence model between the various works since all kinds of RANS approaches were proposed at least once, including the one-equation modeling and all the most common formulations of the two-equation models, as well as an application of DES and LES modeling. Moreover, in the strategy for the near-wall treatment both the Wall Functions and the Low Reynolds approaches were implemented. On the other hand, the numerical settings are almost assessed: the preferred algorithm for the pressure-velocity coupling is the transient SIMPLE (easier settings, good stability, standard solution for the Fluent® code), while the discretization of the N-S equations is mainly based on a 2nd order scheme, both for the time and the spatial derivatives (the upwind scheme is preferred, due to a good compromise between stability and accuracy).

The choices for time-dependent solution parameters show again uncertainty on the values needed to achieve a proper accuracy: the angular time-step ($\Delta\vartheta$) is ranging from 1/15° to 2° depending on the specific application, while the revolutions completed by the rotating region in order to reach a stable and a repetitive torque profile vary from 4 to about 15. As a general indication, the most exploited convergence criterion in the literature is to compare the average value of the torque over a complete rotation between two subsequent revolutions; in most of the works, simulations are stopped when this difference becomes lower than 1%.

The overall domain dimensions used in the majority of the studies are comparable to the usual values for a free flow around an obstacle, being proportional to the size of the obstacle itself (in this case, the rotor diameter D). Both the inlet and the lateral boundaries are placed at a distance (L_1 and W) from the rotational axis of the turbine of about 5-10 diameters, while the outlet boundary at a distance (L_2) of 10-20 diameters. Only one exception [15] conflicts with the global trend, characterized by an overall domain length of about 100 diameters and a width of 80 diameters. It has to be noticed that the simulations can be performed for a turbine placed either in an open field or inside a wind tunnel for the validation with experimental data, determining in the latter case a constraint for the domain width. Finally, the diameter of the rotating region (D_{RR}) is always smaller than twice the rotor diameter, in order to reduce the computational resources needed in performing the mesh motion.

The final section of the comparative literature survey was dedicated to the analysis of the mesh settings, whose properties heavily affect the accuracy and predictability of the results.

In particular, in the near-blade region a suitable resolution of the mesh in the direction orthogonal to the solid walls is conventionally recommended to properly compute the boundary layer profile (y^+), while the number of

nodes in which the airfoil is discretized (N_N) is crucial for the determination of both the incidence angle of the incoming flow on the blade and the boundary layer evolution from the leading edge to the trailing edge. Moreover, the discretization level adopted in the near-blade region also controls the total number of mesh elements (N_E), since the growth rate of the element's size must be small enough to avoid discontinuities.

Upon examination of Table 1, it is readily noticeable that most of the analyzed studies chose a direct resolution of the boundary layer profile, with y^+ values essentially lower than 5. Notwithstanding this, the resolutions of both the blade profile and the global computational domain can vary by more than one order of magnitude and the strategies implemented cannot be standardized since a common rule cannot be found. The elements type used for the grid generation is also not shared: both structured (quadrilateral elements) and unstructured (triangular elements) meshes were applied and an extrusion of layers of quadrilateral elements in the near-wall zone is alternatively used.

3. Study case

A reference rotor for the study was first selected. Thanks to the possibility of exploiting a real full-scale model of an industrial rotor [40]-[41] for the experimental validation, the geometry considered in the study is summarized in Table 2.

The turbine had three very long straight blades (Aspect Ratio higher than 12), realized with an extruded aluminium technology which allowed a very accurate reproduction of the airfoils' geometry. Moreover, rectangular end-plates with rounded off angles were added at the end on each blade in order to further mitigate the tip-losses. Each blade was supported by two airfoil-shaped struts and a central thin tie-rod, which connected it to a steel central shaft with a very small diameter (less than 0.05 m), in order to minimize the shadowing effect on the downwind blades.

It is worth pointing out that, based on the indications by Migliore [44], the geometric airfoils tested onboard the model were cambered profiles, obtained by a conformal transformation of the NACA0018 section by the turbine's radius to compensate the flow curvature effects [41].

As the test model was a pre-industrial prototype of a real machine, no images of the rotor can be shown here due to a non-disclosure agreement with the industrial partner.

The turbine was tested in a large fully open-jet wind tunnel in Italy, able to provide an oncoming flow velocity in the testing section up to 70 m/s, with a flow distortion in terms of velocity variation lower than 0.5% [40]-

[41]. The testing section was more than 8 times larger than the front area of the rotor, whereas the jet length was more than 5 times the turbine's diameter. As the flow can pass around the object freely, this tunnel type is thought to avoid any blockage effect on models up to two times larger than the present rotor, even if supposed to be totally solid. Although proper blockage corrections for VAWTs in open wind tunnels are presently missing, the authors have, however, estimated that blockage can be here neglected based on analogies with some literature works on open-jet wind tunnels [42]-[43].

Both numerical simulations and experimental tests were performed with an undisturbed wind speed of 8 m/s, corresponding to local Reynolds numbers on the blades in the order of $2 \cdot 10^5$.

The rotating axis was connected to an electric motor/brake, which was used to explore the entire power curve of the machine. The torque output and the turbine revolution speed were measured with a high precision torque meter inserted between the shaft and the pulley of the driving belt: the torque meter had a full-scale of 100 Nm with an accuracy of 0.1% of the FSO.

In particular, in order to obtain experimental data that could be coherently compared with those coming from 2D simulations, the net torque of the blades was calculated by purging the global torque output from the parasitic torque contribution of the rotating struts and the tower, whose torque was measured in a second run after the blades were removed.

4. Main simulation settings

An extended sensitivity analysis for the assessment of the proper numerical setup was carried out, aimed at highlighting the influence of some critical issues for an accurate two-dimensional simulation of a Darrieus VAWT.

Some preliminary choices were first made on the basis of literature indications. In particular, the simulations were based on a 2D unsteady calculation of the turbine operating in an open field and performed with the ANSYS® Fluent® software package [45].

The unsteady approach required the division of the simulation domain into two sub-domains in order to allow the rotation of the machine. More specifically, the following zones were defined:

- a circular inner zone containing the turbine, rotating with the same angular velocity of the rotor;
- a rectangular fixed outer zone, determining the overall domain extent.

The introduction of a conservative circular sliding interface, defined by the diameter of the rotating region (D_{RR}), guaranteed the connectivity between the two separated regions as well as the relative motion of the components. For the definition of the rotor geometry, only the turbine's blades were taken into account, neglecting the presence of both the supporting struts and the shaft.

The main parameters of the fixed area are shown in Figure 1: the velocity inlet and pressure outlet boundary conditions were placed respectively at a L_1 distance upwind and L_2 distance downwind with respect to the rotational axis of the turbine, while a symmetry condition was assigned to the lateral boundaries, identified by the width W. The symmetry condition for lateral boundaries is indeed the most common solution for this type of simulations (see literature survey). An alternative option, however, could be represented by "opening-type" conditions (i.e. able to support simultaneous inflow and outflow over a single region), which could enable a reduction of domain width. Due to possible instabilities generated by this type of setting, however, in this work the conservative choice of symmetry conditions was maintained.

Due to the remarkable influence of the domain sizes on the correct description of the flow field past the turbine, a specific analysis on these parameters was carried out, whose results will be discussed later in the study.

The 2nd order upwind scheme was used for the spatial discretization of all the equations including a transport term (i.e. momentum, energy and turbulence), as well as the bounded 2nd order implicit for the time differencing, to achieve a good resolution. In order to ensure a stable simulation, the initialization of the solution was performed by first calculating the steady-state flow around the rotor, obtaining an initial guess for the unknown variables. Then, the time-dependent simulation started with a 1st order differencing scheme in both time and space, switching only after few revolutions to the 2nd order scheme.

As indicated by the literature, a converged solution was achieved by running the simulations until a periodic behavior was reached; the global convergence was monitored comparing the average value of the torque over a complete revolution between two subsequent revolutions. Contrary to the literature, however, the sensitivity of the results on the selected threshold for torque assessment was specifically investigated in this work (see Section 4.2).

Beyond these basic assumptions, however, the lack of agreement in the technical literature led this study to investigate the following parameters within the indicated ranges:

- Turbulence model: Standard k-ε, RNG k-ε and k-ω SST
- Solver type: pressure-based, density-based

- Fluid properties: compressible, incompressible
- Solution Algorithm: SIMPLE, PISO, *Coupled*
- Angular time-step: 0.27°, 0.9°
- Iterations per timestep: 20, 30, 40
- Domain dimensions: L_1, L_2, W
- Number of revolutions to convergence: variable with the tip-speed ratio

It is worth pointing out that all the considered variables not only directly affect the accuracy of the final result but also have a strong mutual influence between themselves; as a result, the analysis tried on one hand to decouple the effects of the variables and, on the other hand, to highlight their influence on other components as well as on the simulation outcomes.

In particular, in the first phase of the study, focused on the assessment of the most effective numerical setting, the boundaries were initially placed very far away from the rotor (similar to [15]), in order to avoid any distortion on the flow field and allow a specific investigation on the parameters affecting the accuracy of the model in describing the flow-blades interaction. Moreover, a reference mesh was created on the basis of the highest refinement level found in the literature [15]. Both these parameters then became part of the analyzed variables. As a general indication, the multivariate matrix of tests obtained with the aforementioned parameters was in fact analyzed, with the exception of those combinations involving elements that were already discarded based on specific evidence. Throughout the study, the general criteria that were used for the evaluation of the acceptability of the results were:

- A satisfactory matching between simulation results and experimental data;
- The achievement of insensitivity to the variation of a parameter;
- The convergence of residuals (all quantities to 10^{-5}, except for momentum to 10^{-6}) and computational limits.

Moreover, it is here proposed that the most correct way of comparing two simulations should be not only based on the comparison between the calculated torque values or torque coefficients, as very often made in the literature. As aggregate parameters, they are in fact deemed to potentially hide differences between the simulations, due to undesired compensations between different zones of the torque profile. On this basis, in the present study the attention was focused both on the averaged power coefficient values over a revolution and on the evaluation of the mean error between the instantaneous torque coefficient profiles.

4.1 Turbulence model

In order to evaluate the influence of turbulence modeling, only two-equation models were tested, by means of an Unsteady Reynolds-Averaged Navier-Stokes (U-RANS) approach.

One-equation models were indeed not taken into account since they are deemed to be poorly predictive in largely separated flows and free shear flows [46].

Three different models were tested and compared: Standard k-ε, RNG k-ε and k-ω SST.

The ε-based models failed in satisfying the convergence requirements, with residual values for the momentum in the order of 10^{-4}. Moreover, poor coherence with experimental results was provided by RNG k-ε, while k-ω SST showed better performance in terms of stability and reliability, as well as the best agreement with experiments.

Finally, since the main requirements were the accuracy in the discretization of the boundary layer and the capability of capturing the stall phenomena occurring on the profile during the revolution, the *Shear-Stress Transport* (SST) k-ω model was chosen to model the turbulence. The *Enhanced Wall Treatment* was implemented for the computation of the boundary layer in the near-wall regions, which introduces a modification in the turbulence model to enable the viscosity-affected region to be resolved up to the wall.

The SST model is based on a zonal formulation, which makes use of blending functions in order to switch from a ω-based formulation inside the boundary layer to a ε-based formulation in the core region of the flow [47]. This model was chosen mainly because it offers the typical advantages of the most used conventional two-equation turbulence models, k-ε and k-ω, avoiding their respective basic shortcomings. In detail, the ε-based models fail to predict the proper behavior of turbulent boundary layers up to separation, while their application is recommended in free shear flows, i.e. jet and wake, mixing layers, etc. On the other hand, the use of ω-based models is suggested for compressible flows and separating flows under adverse pressure gradients, although they reveal strong sensitivity of the solution on arbitrary freestream values of both k and ω outside the shear layer ([46], [48]-[49]). Moreover, the calibration of the SST model was originally focused especially on smooth surfaces [45].

In the case of a real Darrieus functioning, both phenomena actually occur, making the k-ω SST approach by far preferable than other solutions.

4.2 Convergence criteria

The usual convergence criterion based on the deviation of the averaged torque value of a blade (or power coefficient) over a complete revolution between two subsequent cycles was here thought to represent the most effective solution to ensure a stable behavior of the simulation.

Contrary to the literature, however, in which the calculations are generally stopped as soon as the difference becomes lower than 1%, a sensitivity study was here carried out.

In particular, it was noticed that the required number of revolutions cannot be estimated *a priori*, being notably dependent on the tip-speed ratio of the turbine. In the study, the minimum number of cycles felt in a range between 20 and 90. For example, in Figure 2, the convergence histories of two simulations at TSR=1.1 and TSR=2.2 with the same settings are reported: the power coefficient was divided by its final value ($C_{P,F}$).

From a perusal of Figure 2, it is readily noticeable that the number of revolutions can substantially vary from an operating point to another. In addition, the 1% threshold appears not suitable for similar simulations as the very flat convergence trend can introduce significant variations in the final torque value. For example, in case of the TSR=2.2 simulation, the deviation of C_P between two subsequent revolutions goes under 1% just after 5 rounds: the value at that cycle (i.e. the one accepted on the basis of literature criteria) would however overestimate the final value ($C_{P,F}$) of about 9%, introducing a non-negligible detriment of the simulations accuracy.

To overcome this limit, the convergence threshold applied in the study was reduced by one order of magnitude and fixed to 0.1% of the C_P value between two subsequent revolutions.

4.3 Solver settings

The assessment of the numerical approach is here discussed. First, some considerations on the effects of compressibility are provided. Then, the attention is focused on the choice of the type of solver and solution algorithm to be used for the simulations, accounting also for the effects of the angular time-step and the number of inner iterations per time step.

Two different revolution regimes were considered for the analysis (TSR=1.1 and TSR=2.2), in order to evaluate the effectiveness of the approach for different working conditions of the machine (i.e. relative wind speeds and ranges of incidence angles); the two functioning points are in fact located in the unstable and stable part of the torque curve, respectively.

Concerning the method for the treatment of the gas density, it is worth pointing out that the flow through a Darrieus turbine is characterized by low Mach number values. Therefore, the effects of compressibility can be considered mild or even null. In these conditions, since the pressure is almost not linked to the density, the most straightforward choice for the solver type is represented by the pressure-based approach, in which the continuity equation is used in combination with the momentum equation to derive an equation for the direct solution of the pressure field.

On the other hand, the application of a density-based approach might not be recommended, as the continuity equation is used as a transport equation for density, while the pressure field is determined from the equation of state ([50]-[51]). Notwithstanding this, recent developments and modifications in the numerical methodologies led to the extension of the applicability of both solvers in order to properly perform for a wider range of flow conditions [45].

On these bases, a comparative analysis was carried out between the two approaches, whose results are not reported here for conciseness reasons. The results demonstrated, however, that the pressure-based approach is more stable and has a faster convergence rate than the density-based one; moreover, due to its intrinsic formulation, this latter approach would require very low residuals and very short timesteps to ensure an accurate solution, which are, however, very hardly achievable in case of large and unsteady simulations like those considered in this study. For example, if one imposes an angular timestep of 0.27° together with 40 iterations per timestep, the residuals were not able to become lower than 10^{-3}. As a result, the pressure-based formulation was selected for the simulations.

The *ideal gas law* was enabled for the required material properties; a sensitivity analysis was indeed carried out also on the proper choice between the formulations for incompressible or compressible flow: the resulting fields of density, temperature and Mach were analyzed. The results demonstrated the absence of appreciable compressibility effects, although a slight overestimation of the power coefficient was observed. The convergence rate was not, however, speeded up by the simpler formulation, i.e. the incompressible law. Therefore, the more complex and accurate model, i.e. the compressible law, was preferred since it was assumed to guarantee a higher degree of detail without additional computing effort.

Finally, since the pressure-based solver was specified, the last requirement was the choice of the algorithm to solve the linkage between pressure and velocity. An iterative solution is in fact needed due to both the non-linearity in the N-S equations set and the lack of an independent equation for the pressure, as mentioned before. The two standard alternative formulations for the pressure-velocity coupling are the *Semi-Implicit Method for*

Pressure-Linked Equations (SIMPLE) and the *Pressure Implicit with Splitting of Operators* (PISO), both based on the solution of an additional equation for the pressure field ("pressure-correction equation"). Originally, the PISO method was preferable for transient problems since it was derived from the SIMPLE one specifically for unsteady calculations: with sufficiently small timesteps, accurate results could be obtained with lower computational costs than the SIMPLE algorithm [50]. Both these semi-implicit solution methods are, however, known to converge slowly since the momentum equation and pressure-correction equation are solved separately [45], i.e. with a segregated approach.

Starting from these considerations, a coupled approach (non-segregated) was tested in addition to SIMPLE and PISO algorithms. In the *Coupled* algorithm, the N-S equations set is directly solved through an implicit discretization of pressure in the momentum equations, with benefits in terms of robustness and convergence, especially with large timesteps or with a poor-quality mesh ([45], [52]).

The worst performance in terms of accuracy of the results was found with the PISO algorithm: an excessive overestimation of the experimental torque was observed for both the simulated regimes. As an example, Figure 3 shows the single blade instantaneous torque coefficient at TSR=1.1 as a function of the azimuthal position during a complete revolution.

The simulated case with the PISO algorithm is compared to the results obtained with the final settings established at the end of the sensitivity analysis, which are more closely matching experimental data: a complete mismatch in the upwind zone of the rotation is clearly visible for the PISO curve, with a peak overestimation of approximately 30%. This behavior is due to a wrong detection of the stall onset, since the flow remains attached to the blade for further 10° of rotation.

The attention was then focused on the comparison between SIMPLE and *Coupled* algorithm. The torque coefficient profile at TSR=2.2 is reported in Figure 4 with azimuthal increments of 0.9° and 0.27° for both algorithms: considering the results with the smaller timestep, the two curves are nearly coincident, indicating an almost equivalent response of the two algorithms. Nevertheless, increasing the timestep to 0.9°, a remarkable difference in the C_T profile can be observed in case of the SIMPLE algorithm, with a 4% overestimation of the power coefficient, while the *Coupled* algorithm shows just a slight modification, with a minimal reduction of the peak value. The lower sensitivity to the temporal discretization (confirmed by many other analyzed cases, not reported here) led to the choice of the *Coupled* algorithm as the preferable and more robust formulation for the pressure-velocity coupling.

The last analyses were addressed to the effects of the number of inner iterations performed for each time step. If the stopping criterion for inner iterations was in fact a threshold level for all the residuals of 10^{-5}, the complex nature of the phenomenon did not allowed to always reach this accuracy for all the variables. In particular, the residuals on the turbulent kinetic energy in specific positions of the rotor were usually higher than the prescribed value.

To overcome this problem, as common practice in this type of simulations, a maximum number of iterations was set as an additional stopping criterion. The best compromise between accuracy and computational cost reduction is therefore to identify the number of iterations needed to ensure that all the other variables are able to reach the prescribed accuracy, with no appreciable variation of the solution.

For example, the results obtained with three different numbers of iterations (20, 30 and 40) are illustrated in Figure 5 at TSR=1.1, using an angular timestep of 0.27° and the *Coupled* algorithm. It is worth pointing out that the timestep of 0.9° was not considered here, since the TSR=1.1 regime is a definitely critical operating point with a highly unstable torque output and therefore the quality of the results with such a large timestep would be very poor. In Figure 5, a variation in the torque coefficient curve can be observed comparing the results with 20 and 30 iterations. In particular, the residuals level reached in the first case is in the order of 10^{-4} for the continuity and 10^{-5} for the momentum. Increasing the iterations number up to 30, all the variables reached a residual level of 10^{-5}, with the only exception of the turbulent kinetic energy. A further increase to 40 iterations did not led to any sensible difference of the C_T profile (i.e. on the solution of each timestep), although the turbulent kinetic energy residual was in the order of 10^{-4}. On these bases, the 30 iterations setting was considered a suitable compromise between accuracy and computational cost.

4.4 Boundaries

The effects of the domain extent on the torque output were finally analyzed. The goal was to place the boundaries at a distance sufficient to avoid any influence on the evolution of the flow field around the turbine. Five different cases (Table 3) were tested at TSR=2.2 by progressively increasing the overall domain length (L) and width (W), keeping a constant aspect ratio of the rectangular stationary region, as well as a constant ratio between the distances of inlet and outlet boundaries ($L_2/L_1 = 2$). The only exception is *Case E*: the domain width was indeed the same of that used in *Case D* while the total length was further increased. All the aforementioned dimensions are reported in a normalized form with respect to the rotor diameter (D).

The trend of power coefficient as a function of the domain length (Figure 6) clearly demonstrates that the typical settings adopted by other authors, except [15], are by far unsuitable for the proposed goal: a C_P overestimation of 14% and 4% is observed for *Case A* and *Case B*, respectively, in comparison with the largest domain. This behavior can be mainly attributed to the blockage effect of the lateral boundaries, where a symmetric condition is applied, i.e. only the axial component of the velocity is allowed.

This phenomenon can be readily appreciated in Figure 7, where the velocity contours in the entire domain are displayed for *Cases B*, *C* and *E*. In *Case B*, the flow is crosswise confined with a non-physical behavior and it is forced to accelerate in the rotor region, thus intensifying the energy extraction. For *Case C*, the overestimation is dropped to 1% but a slight influence of the lateral boundaries can be still noticed in Figure 7: the bulk velocity in the downwind region is in fact higher than in the upwind zone. Moreover, the outlet boundary is placed at a distance where the turbine's wake is still marked, while it is preferable to allow a complete development. The comparison of *Case D* and *Case E* ensures the attainment of the insensitivity to the domain extent, with a deviation of less than 0.3%: the wake is completely dissipated and the flow condition in correspondence of the boundaries is essentially uniform.

As a result of the first part of the study, a baseline set-up was defined with the following properties:

- Turbulence model: *k-ω SST*
- Solver type: pressure-based
- Fluid properties: compressible
- Solution Algorithm: *Coupled*
- Iterations per timestep: 30
- Domain dimensions: $L_1 = 40D$, $L_2 = 100D$, $W = 60D$

5. Sensitivity analysis on spatial and temporal discretization

Once the main simulation settings have been assessed, the right choice of both the spatial and the temporal discretizations becomes the key point for a successful simulation.

In particular, while in common RANS simulations the attention is primarily focused on ensuring a sufficiently refined mesh (spatial discretization), in the present case the sudden variation of the flow conditions on the airfoil during the revolution imposes a specific analysis of the temporal discretization. More specifically, the azimuthal

increment between two subsequent steps of analysis must be small enough to correctly describe every flow structure (vortices, wakes, etc.) that is originated in the flow field; otherwise, significant errors could be introduced in the predicted torque profile over a revolution.

Moreover, it is worth remarking that a strong mutual influence is established between the temporal and spatial characteristic scales; in order to accurately describe a structure, e.g. a dynamic-stall vortex, it is in fact important both a fine mesh, to capture the gradients, and a very small advance of the rotating frame, to avoid any undesired discontinuity of the variables between two instants.

On these bases, a multivariate sensitivity analysis was carried out accounting for the mesh features and the timestep. In addition, a check on the number of inner iterations needed for each timestep was constantly ensured, confirming, however, that 30 iterations were generally sufficient to a stable solution also in the most critical functioning points.

5.1 Analysis parameters

Table 3 reports the characteristics of the investigated meshes. The first two meshes (G1 and G2) were generated based on the settings of the coarsest examples found in the literature: their poor refinement levels, however, were clearly marked as unsuitable for the present application and the results obtained are not shown here for conciseness reasons. The inconsistency of the results is mainly related to a poor capability in capturing the stall development, being greatly anticipated especially using a mesh without an extrusion of quad layers (G1), and to y^+ values between 10 and 40 with the G2 mesh, falling in the range of the buffer layer, i.e. outside the limits of applicability of both a wall function approach and a direct resolution of the boundary layer. The original mesh used to assess the numerical scheme discussed in the previous section was G4: from it, a coarser (G3) and two finer (G5 and G6) meshes were originated.

The main parameters used to control the final mesh size were the resolution of the airfoil profile, by varying the number of grid points (N_N) and the resolution of the boundary layer, by varying progressively the rows' number of quadrilateral elements (N_{BL}) as well as the first row thickness (y_P).

As an example, Figure 8 shows some details of the G4 mesh: (a) stationary domain, (b) rotating domain, (c) near-blade region, (d) leading edge of an airfoil, (e) trailing edge of an airfoil.

The mesh performance was evaluated at three different regimes, i.e. TSR values of 1.1, 2.2 and 3.3, respectively. As already discussed, a specific analysis at different operating points is of particular interest as the operating conditions of the airfoils can be substantially modified due to the different range of incidence angles

which also affects the development of unsteady phenomena like the dynamic stall [9]. The influence of the timestep was included by initially accounting for three angular increment sizes ($\Delta\vartheta$=0.135°, 0.27° and 0.405°): moreover, when the final spatial discretization had been assessed, a specific trend was highlighted between the required timestep and the revolution speed of the rotor, as will be shown later in the study.

The evaluation criteria to define the mesh performance were:

- A satisfactory matching between simulation results and experimental data
- An effective independence of the results from the elements number in the mesh
- The achievement of proper values of the y^+ and the Courant Number (Co)

More specifically, a y^+ value in the order of ~1 was considered as the target for the *enhanced wall treatment* approach ([47], [45]), to satisfy the typical resolution requirements to capture the viscous sub-layer. On the other hand, an in depth analysis was added on the Courant Number, which had been not always properly considered in the literature. Due to the very high number of tests deriving from the aforementioned considerations, only some results of particular interest are reported here, while general trends are shown and discussed.

5.2 Results: torque profile

First, Figure 9 reports the comparison of the single blade torque coefficient over a revolution at TSR=1.1. This regime is particularly critical as the incidence angles experienced by the airfoil are very high and large separated regions occur due to airfoils stall.

The base mesh G4 is compared to the finest one (G6) with azimuthal increments of 0.27° and 0.135°.

Upon examination of the figure, a very good agreement is readily noticeable between the results with the only exception of the G4 mesh with the coarser azimuthal angle: with this setting, the flow detaches too early in the upwind zone (approximately at ϑ=60°) and the generated vortices remarkably alter the downwind torque extraction. As previously discussed, this notable difference in the turbine functioning would have been barely appreciable if one would have focused the attention only on the power coefficient for which a difference of approximately 2.5% of the final value is noticed.

This behavior can be observed in Figure 10, where the vorticity field is plotted for four relevant positions (indicated in Figure 9) of the blade during the revolution.

The results of the simulation with the G4 mesh and an angular timestep of 0.27° is compared to the most accurate case, i.e. G6 mesh with angular timestep of 0.135°. Starting from position A, the onset of a recirculating zone is clearly distinguishable on the leading edge of the G4 mesh, while the boundary layer is completely

attached in the G6 mesh. This phenomenon notably affects the following evolution of the vortex structures, especially in the second quadrant (position B), where the recirculating zone close to the blade tends to move forward the leading edge instead of expanding laterally. On the other hand, the vortex shapes are nearly equivalent in the third quadrant (position C).

Finally, the pronounced difference in the fourth quadrant can be explained by examining position D: the lower torque output obtained with the G4 mesh in the angular range 300°-360° is due to the higher intensity and proximity of the main vortex generated by the stall in the upwind region, while the higher torque in the range of 240°-300° is mainly due to the absence of a secondary vortex weakening the pressure side of the profile.

Following the same criterion, the complete sensitivity analysis at TSR=1.1 is reported in Figure 11 in terms of power coefficient as a function of the cells number in the rotating domain.

Figure 11 clearly shows that, at this regime, an azimuthal angle of 0.27° is not sufficient to guarantee a reliable estimation of the torque extraction, except in case it is coupled with a very fine mesh. On the other hand, by reducing the timestep, a more stable trend is obtained with a consistent torque output.

Moving towards a more stable functioning point, where the flow is attached for most of the revolution, Figure 12 reports the comparison between the torque coefficient profiles at TSR=2.2 of a blade with all the considered meshes and a timestep of 0.27°: in this case, it is indeed worth pointing out that this azimuthal increment was sufficient to ensure an accurate results as no variation was noticed after a reduction to 0.135°.

An impressive agreement was found between all the considered meshes, with the only exception of G3, which showed a sudden torque coefficient decrease after the peak and, consequently, a completely different oscillation, resulting in a standard deviation even higher than the average value.

To analyze this inconsistency, Figure 13 reports a comparison between the pressure fields obtained with the G3 and G4 meshes relative to four positions of the blade during the revolution (indicated in Figure 12). Considering position A, where the torque is slightly decreasing, the suction side with the G3 mesh exhibits a more extended zone of low pressure, stretching towards the trailing edge. This depression degenerates in the separation of the boundary layer with the generation of a stall vortex that produces substantial variations in the pressure distribution around the blade, especially in the second and third quadrants (positions B and C). This behavior was deemed to be unphysical [9] since the range of incidence angle experienced by the blade for a TSR of 2.2 is limited to very small values, thus avoiding the occurrence of stall phenomena, as predicted by mesh G4.

Finally, in the downwind region where the torque output is approximately zero, the differences are less pronounced, with almost no distinction between the pressure and the suction sides.

In conclusion, a discretization of the blade profile with roughly 100 elements along the chord (227 total elements) is not enough accurate to capture the separation point of the boundary layer.

As a confirmation, the complete sensitivity analysis at TSR=2.2 is reported in Figure 14 in terms of power coefficient as a function of the global cells number.

An almost total insensitivity of the results was yet noticed with $\Delta\vartheta$=0.27° and the G4 mesh, giving an *a posteriori* validation also to the initial assessment of the numerical scheme which was cagily carried out with this setting.

Finally, the highest functioning regime of TSR=3.3 was investigated. Even this regime showed that no differences were introduced by a further decrease of the initial timestep of 0.27° with any of the most refined meshes (G4, G5 and G6). Based on this evidence, an attempt was made in increasing the timestep, which was fixed at 0.405° (i.e. proportionally increased as a function of the revolution speed starting from the 0.135° at TSR=1.1). Figure 15 reports the comparison between the torque coefficient profile of a single blade with G4 and G5 meshes and azimuthal increments of 0.27° and 0.405°: G6 results were not included in the graph because perfectly matching those already presented.

Upon examination of Figure 15, one can easily notice that the G4 mesh is yet by far sufficient to ensure accurate results with both the base timestep of 0.27° and the increased one (0.405°).

In particular, a specific analysis was carried out on the rotor at all the simulated revolution speeds (see validation section), confirming that, with a sufficiently refined mesh, the minimum required timestep for the simulation is constant in time (in the present case equal to $2.25 \cdot 10^{-4}$ seconds), hence proportionally variable with the revolution speed in terms of swept angular sector.

This was indeed a quite unexpected result from an aerodynamic point of view, as the angular spacing was instead considered as the most relevant issue for correctly describing the flow field evolution.

5.3 Results: y^+ and Courant Number

A more in-depth understanding of this phenomenon can be, however, achieved by examining the two main variables describing the quality of the numerical modeling of the flow, i.e. the dimensionless wall distance (y^+) and the Courant Number (Co). If it is commonly agreed that a y^+ value in the order of ~1 can be assumed as a suitable target for the *enhanced wall treatment* ([47], [45]), specific analyses on the Cell Courant Number (Eq. 1) ranges are not so common.

$$Co = V \frac{\Delta t}{\Delta x} \tag{1}$$

Based on its formulation, the number expresses the ratio between the temporal timestep (Δt) and the time required by a fluid particle moving with V velocity to be convected throughout a cell of dimension Δx. While in case of explicit schemes for temporal discretization the Courant-Friedrichs-Lewy (CFL) criterion imposes a limit on the maximum allowed value of Co (i.e. $Co<1$ [51], [53] and [54]) to ensure the stability of the calculation, implicit methods are thought to be unconditionally stable with respect to the timestep size ([45] and [51]).

Although theoretically valid if the problem is studied with a linear stability analysis, when the timestep is increased non-linearity effects would become prominent and oscillatory solutions may occur. On these bases, the literature indicates that an operational Co between 5 and 10 for viscous turbomachinery flows, solved with an implicit scheme, provides the best error damping properties ([53] and [54]).

Recently, an interesting analysis on the application of the CFL criterion to unsteady simulations of Darrieus turbines was presented by [24], which focused the attention on the rotating grid interface; in particular, the satisfaction of an upper bound of 0.15 for the Courant Number in the interface cells is assumed to define the maximum required angular timestep in order to obtain accurate results.

In the present study, a specific analysis was instead carried out on the Courant Number conditions in proximity of the blades, as a correct description of the flow in these zones was in fact deemed to be the most restrictive requisite to accurately predict the torque output; a verification on the conditions at the interface was however made, obtaining Co values very close to the limit suggested by [24].

First, a check on both the y^+ and the Courant Number was made on all the analyzed cases (in terms of mesh, timestep and revolution speed). The y^+ (average and maximum value) was calculated on the airfoil surface, whereas the Co (average and maximum value) was evaluated in three different zones around the blades, comprehended within a distance from the wall of 1, 5 or 10 mm, respectively.

For conciseness reasons, only selected results are reported here. Analogous to the mesh sensitivity analysis, specific attention was paid to the TSR=1.1 regime, which showed the most critical behavior in terms of flow conditions of the airfoils. In particular, Figures 16 reports the average values of the y^+ for the analyzed meshes: in this case, the timestep is arbitrary as it definitely does not affect the calculated flow velocity in the boundary layer. Upon examination of Figure 16, it is readily noticeable that the prescribed limit was always satisfied, indicating that all meshes had a suitable spatial discretization in the orthogonal direction from the blade wall.

Figure 17 conversely shows the average Courant Number within the first region (<1 mm from the blade wall, i.e. the most critical one) over a revolution with G4, G5 and G6 meshes and angular timesteps of 0.135° and 0.27°.

All the analyzed configurations respected the general prescription of $Co<10$. If very fine spatial discretization are used (e.g. G6), the timestep must be likewise reduced to contain the Courant Number, whereas, as expected, the coarsest mesh (G4) is that ensuring the highest degree of stability (minimum Co).

Based on the above the following observations were made:

- The G4 mesh is a very suitable choice for the present study case as it offers sufficient accuracy (see Figures 9, 12, 15), an affordable computational effort and good stability (Figure 17).
- This solution must be, however, coupled with a proper management of the timestep as a function of the revolution speed of the rotor: in detail, when the revolution regime decreases, the azimuthal increment between two subsequent steps must be proportionally reduced to ensure both a good accuracy (see Figures 9, 12, 17) and a proper stability of the calculation.
- Only in case of very low revolution speeds, were the airfoils experience very unstable functioning conditions, the use of finer meshes can be considered in order to enhance the accuracy of the simulation (Figure 11).

Within these assumptions, the analysis was further focused on a more in-depth evaluation of the results obtained with the G4 mesh. In particular, a global check on the suitability of the dimensionless parameters was carried out for the three reference revolution regimes of TSR=1.1, TSR=2.2, TSR=3.3 and their corresponding angular timesteps. In particular, Figure 18 and Figure 19 report the average and maximum values of the y^+ as a function of the azimuthal position, respectively.

Upon examination of the results, it is readily noticeable that the mesh properties in the near-wall region were correctly defined since the average values of y^+ were all around the limit of 1 that represented the target of the simulations, although a small (acceptable) increase is observed, due to the increase in the relative flow velocity, hence the wall shear stress. Moreover the same increase was not observed for the maximum values of y^+, ensuring similar values (in the order of 3.5) for all regimes, which were registered only in very few cells of the domain.

At the same time, Figure 20 and Figure 21 report the average and maximum values of the Courant Number over a revolution, respectively. With the selected settings, the average Courant Number (Figure 20) was always contained within 5.0, i.e. by far lower than literature prescriptions ([53] and [54]); a slight increase of the average value is however observed, nearly proportional to the revolution speed which makes the relative velocity (V) increase while both Δx and Δt remain constant (see Eq. 1).

On the other hand, the choice of having a constant timestep in time (i.e. an angular timestep increasing with TSR) made the maximum *Co* values collapse approximately on the same trend, with a peak in the order of 40, definitely acceptable as referred to a very limited number of cells.

Based on these results, despite the generally high computational resources required, the selected settings were then assumed to represent the best compromise able to ensure accurate results of the simulations.

6. Validation and discussion

In order to assess the validity of the proposed numerical modeling, different validations were carried out.

First, CFD simulations with the described settings were compared to the power coefficient data of the rotor obtained with the wind tunnel campaign. As discussed, this validation was indeed of particular interest as the experimental data had been purposefully collected to represent a valid test case also for a 2D simulation (blades with high aspect ratios and purging of the parasitic torque). Moreover, the possibility of exploring the entire power curve was functional to the validation of the differentiated numerical settings with the operational regime of turbine.

A further assessment of the reliability of the proposed approach was achieved by applied the numerical settings to the simulation of the rotor tested by Raciti Castelli et al. [5]. The analysis, whose details are reported in [55], revealed the CFD approach was able to reproduce the experimental peak power coefficient with an error lower than 4%. Moreover, the proposed numerical approach was also assessed in comparison to a research numerical code.

As a second step, the need of validating the prediction accuracy of instantaneous torque led to the selection of one of the most reliable experimental data set available in literature. In detail, the experiments by Laneville e Vittecoq [9]-**Errore. L'origine riferimento non è stata trovata.**, were analyzed in terms of torque coefficient over a revolution.

6.1 Power curve comparison with experimental data

Figure 22 reports the comparison between simulated data and experiments in terms of power coefficient vs. TSR.

Very good agreement is readily noticeable almost in every point of the functioning curve of the turbine. Such an impressive match between the two data sets was probably favored by the fact that the experimental data were

purged from the tare torque and the blades of the rotor were long enough (AR>12) to reduce the influence of the tip-losses. An only partial discrepancy was noticed in correspondence of the curve peak, where CFD overestimates the C_P; this phenomenon is probably due to a different modeling of such a difficult condition, in which the experienced incidence angles range becomes narrow enough to modify the dynamic stall characteristics, or even suppress its onset, with a consequent variation of torque extraction in the second quadrant. Notwithstanding this, properly settled CFD analyses can be definitely considered fully representative of the turbine behavior and can be then further exploited in the near future to analyze specific aerodynamic problems connected to its functioning.

On the other hand, a not-optimized setting of the simulation can substantially modify the prediction accuracy. For example, a comparative analysis was carried out aimed at estimating the effects of the most common issues analyzed in this study on the performance estimation accuracy of CFD. In detail, three non-optimized configurations were selected and tested on some selected TSR conditions:

- CONFIGURATION 1 – Representative of an insufficient domain width. Simulations were carried out with the dimensions defined for Case B in Table 3.
- CONFIGURATION 2 – Same settings of the optimized simulation but with a convergence criterion using a threshold on the torque output of 1% with respect to the previous revolution (literature criterion).
- CONFIGURATION 3 – Example of a temporal discretization optimized using only one point of the curve. In the selected case, a timestep of 0.405° (anyhow lower than the majority of literature proposals) was used in all the operating points as if one would have been identified it only based on the sensitivity analysis at TSR=3.3.

The main outcomes of the comparative analysis are presented in Figure 23.

Upon examination of the results, it is readily noticeable that non-optimized settings can notably affect the accuracy of the torque prediction. In particular, small domains (Configuration 1) generally force the flow to remain attached to the blades beyond the real condition, thus inducing a spread overestimation of the turbine performance.

The common convergence threshold in the order of 1% of the torque between two subsequent revolutions does not guarantee accurate solutions, especially at high revolution speeds, where the flow is attached to the airfoils for most part of the revolution and hence a correct evaluation of the flow conditions becomes crucial.

The use of a sufficient temporal discretization is one of the relevant issues for an accurate simulation of rotating machines. In case of Darrieus rotors, low tip-speed ratios generally require lower angular timesteps in

order to correctly describe the flow structures originated due to separations in correspondence of high angles of attack.

In particular, the proposed analyses are thought to have highlighted some of the most important issues in correctly describing Darrieus VAWTs with CFD and a coherent approach to assess them. The identified numerical values, however, have to be considered as representative only of the present study turbine and must be properly scaled in case of different turbine dimensions or airfoil's characteristics.

6.2 Instantaneous torque comparison with literature data

Reliable experimental results on the instantaneous torque output of a Darrieus rotor are extremely rare in technical literature. The most complete and accurate data set available is probably that reported by Vittecoq and Laneville [56], which was also exploited by Paraschivoiu for the assessment of dynamic stall models in BEM codes [9]-[56]. In the experiments, a two-bladed H-Darrieus rotor was tested, whose main features are reported in Table 5.

As the experiments were particularly focused on the evaluation of instantaneous torque, the resistant torque of the struts was minimized by using two guitar chords to connect the blades to the centrals shaft. The accuracy of airfoils' shape and finishing was controlled with an optical comparator. A very accurate acquisition system was provided, whose detail can be found in Ref. [56].

The rotor was tested in the wind tunnel of the University of Sherbrooke (Quebec, Canada). All the tunnel walls were removed for an open-jet configuration. At the turbine location, the section area was 1.82 m x 1.82 m [56]. The turbine axis was placed at 0.65 m from the tunnel outlet [57].

Based on the above, the numerical set-up of simulations was slightly modified to account for the jet effect connected to the specific layout of the tunnel. In detail, the inlet of the domain was limited to a section of 1.82 m and get near to the turbine at the prescribed distance of 0.65 m. Both the lateral and the downwind boundaries were instead maintained at distances of 60D and 100D, respectively.

In order to assess the proper spatial and temporal discretizations, a preliminary analysis of the rotor was carried out with a proprietary BEM code [58]-[59], as no information on the power coefficient curve was provided in the reference. The code revealed that the proposed rotor is credited of a very poor performance at the considered wind speed (i.e. U=3.2 m/s) with an almost null power coefficient. In these conditions, despite the TSR equal to 3.0, the rotor was simulated as if working in an unstable regime. In further detail, the two NACA0018 airfoils were discretized with a mesh comparable to the original G6, i.e. approximately 1800 nodes on the airfoil,

$9.0*10^5$ elements in the rotating region and y^+~1. Moreover, in order to ensure a correct evaluation of flow separation and vortices propagation, a small timestep was preferred, equal to 0.15°.

Figure 24 reports the comparison between simulations and experiments in terms of instantaneous tangential force coefficient (C_{tang}) along revolution for a declared revolution speed of 300 rpm and a TSR=3.0.

Despite the uncertainties connected to the experiments and the highly complex functioning point (average C_{tang} almost zero), the agreement is impressively good, confirming that the proposed computational approach can effectively reproduce the physics of Darrieus wind turbines, opening interesting prospects for future analyses based on CFD.

7. Conclusions

In the present study, an extended analysis was carried out to highlight some critical issues for an accurate two-dimensional CFD simulation of Darrieus wind turbines.

All the choices made in the study concerning each of the main numerical parameters of the model were based on specific comparative analyses, which assessed the influence of the parameter itself both on the solution stability and on the accuracy with respect to purposefully collected experimental data on the study turbine. Moreover, a literature case study also confirmed the suitability of the proposed numerical approach also for the prediction of the instantaneous torque profile of a Darrieus turbine.

From experience of the present study, the following indications are proposed:

- The pressure-based solver using a coupled algorithm for a compressible flow is thought to represent the best numerical approach, if combined with the 2nd order upwind scheme for the spatial discretization of all the transport equations and the bounded 2nd order implicit for the time differencing.
- The *k-ω SST* turbulence model is the most suitable choice for the simulation of Darrieus turbines functioning, which contemporarily involves the presence of both boundary layer separation and free-shear flows.
- A convergence criterion based on the variation of the torque output can be a valuable solution but only on condition that a very strict threshold is imposed. In detail, the convergence history of the simulations revealed that, although a torque variation lower than 1% (i.e. the value generally adopted in the literature) between two subsequent revolutions is generally achieved after only few cycles, the torque value measured after this threshold can be sensibly different (up to approximately 10%) from the final value at

convergence. A convergence criterion is then proposed using a limit on the torque variation lower than 0.1%.

- The domain dimensions to ensure an open-field-like behavior of the rotor must be extended significantly with respect to what is generally suggested in the literature. In the present case, the results insensitivity to boundaries' distance was obtained by placing the inlet section 40 rotor's diameters upwind the center of the turbine, the outlet section 100 diameters downwind and each lateral boundary 30 diameters away. Moreover, to avoid undesired disturbances generated at the sliding interface, the rotating region had a double diameter with respect to the turbine.
- A specific mesh region for boundary layer resolution can provide notable advantages in terms of accuracy, on condition that y^+ values in the order of 1 are guaranteed. This simulation cases generally require very heavy meshes, particularly due to the high number of nodes needed on the airfoils' surface. The refinement level must be further increased in case of low tip-speed ratios of the rotor, where the large incidence angle variations make a correct localization of the stall point on the profiles even more important.
- The study showed that the required temporal discretization is almost independent on the revolution regime considered for the simulation. In detail, a constant timestep was identified which allowed to contain both the average and the maximum Courant Number in proximity of the blades. As a result, the angular timestep becomes directly proportional to the revolution speed of the rotor. In the present case study, angular timestep in the range between 0.135° and 0.405° were used. Small angular timesteps are also suggested in case of low wind speeds were the torque output of the rotor is reduced and large separate regions occur.

The good prediction capabilities shown by the simulations using the proposed set-up confirmed that a properly assessed two-dimensional approach is definitely able to describe the actual functioning of Darrieus rotors, hence providing a very useful tool to analyze several aerodynamic phenomena not yet completely understood, like dynamic stall and flow curvature effects.

8. Acknowledgments

Thanks are due to Prof. Ennio Antonio Carnevale of the University of Florence for his support in this study.

9. Nomenclature

Acronyms

AR	Aspect Ratio

BEM	Blade Element Momentum
CFD	Computational Fluid Dynamics
CFL	Courant, Friedrichs and Levy criterion
DES	Detached Eddy Simulation
FSO	Full Scale Output
LES	Large Eddy Simulation
N-S	Navier-Stokes
PISO	Pressure Implicit with Splitting of Operators
RANS	Reynolds-Averaged Navier-Stokes
RNG	Re-Normalization Group
SIMPLE	Semi-Implicit Method for Pressure-Linked Equations
SST	Shear Stress Transport
TSR	Tip-Speed Ratio
U-RANS	Unsteady Reynolds-Averaged Navier-Stokes
VAWT	Vertical-Axis Wind Turbine

Greek symbols

α	Incidence Angle	[deg]
$\Delta\vartheta$	Azimuthal Angle Increment	[deg]
Δt	Temporal Timestep	[s]
Δx	Cell's Dimension	[m]
ε	Turbulence Dissipation Rate	[m^2 s^{-3}]
ϑ	Azimuthal Angle	[deg]
σ	Turbine's Solidity	
ω	Specific Turbulence Dissipation Rate	[s^{-1}]
Ω	Turbine's Revolution Speed	[rpm]

Latin symbols

c	Blade's Chord	[m]
C_P	Power Coefficient	

$C_{P,F}$	Power Coefficient at Convergence	
C_T	Torque Coefficient	
C_{tang}	Tangential Force Coefficient	
Co	Courant's Number	
k	Turbulence Kinetic Energy	[m^2 s^{-2}]
r	Turbine's Radius	[m]
y^+	Dimensionless Wall Distance	
y_P	Height of the First Element in the Boundary Layer	[m]
D	Turbine's Diameter	[m]
D_{RR}	Rotating Region Diameter	[m]
L	Domain Total Length	[m]
L_1	Distance between the Inlet Boundary and the Turbine	[m]
L_2	Distance between the Turbine and the Outlet Boundary	[m]
N	Blades' Number	
N_N	Number of nodes on blade profile	
N_E	Total number of mesh elements	
N_{ER}	Number of mesh elements in the rotating domain	
N_{ES}	Number of mesh elements in the stationary domain	
R	Turbine's Radius	
rev	Revolutions to convergence	
U	Wind Speed	[m/s]
V	Velocity	[m/s]
W	Domain Width	[m]

10. References

[1] S. Mertens, Wind Energy in the Built Environment, Multi-Science, Brentwood (UK), 2006.

[2] E. Dayan, Wind energy in buildings: Power generation from wind in the urban environment - where it is needed most, Refocus, 72 2 (2006) 33-38.

[3] F. Balduzzi, A. Bianchini, E.A. Carnevale, L. Ferrari, L., S. Magnani, Feasibility analysis of a Darrieus vertical-axis wind turbine installation in the rooftop of a building, Applied Energy. 97 (2012) 921–929.

[4] F. Balduzzi, A. Bianchini, L. Ferrari, Microeolic turbines in the built environment: influence of the installation site on the potential energy yield, Renewable Energy. 45 (2012) 163-174.

[5] F. Toja-Silva, A. Colmenar-Santos, M. Castro-Gil, Urban wind energy exploitation systems: Behaviour under multidirectional flow conditions - Opportunities and challenges, Renewable and Sustainable Energy Reviews. 24 8 (2013) 364-378.

[6] T. Sharpe, G. Proven, Crossflex: Concept and early development of a true building integrated wind turbine, Energy and Buildings. 42 12 (2010) 2365-2375.

[7] A. Bianchini, G. Ferrara, L. Ferrari, S. Magnani, An improved model for the performance estimation of an H-Darrieus wind turbine in skewed flow, Wind Engineering. 36 6 (2012) 667-686.

[8] M. Borg, M. Collu, F.P. Brennan, Offshore floating vertical axis wind turbines: advantages, disadvantages, and dynamics modelling state of the art, Marine & Offshore Renewable Energy Congress, London (UK), 26-27 September, 2012.

[9] I. Paraschivoiu, Wind Turbine Design with Emphasis on Darrieus Concept, Polytechnic International Press, Canada, 2002.

[10] M. Islam, D.S.-K. Ting, A. Fartaj, Aerodynamic models for Darrieus-type straight-bladed vertical axis wind turbines, Renewable and Sustainable Energy Reviews. 12 4 (2008) 1087-1109.

[11] J.H. Strickland, The Darrieus Turbine a Performance Prediction Model Using Multiple Streamtubes, Sandia National Laboratories, Technical Report No. SAND75 0431, 1975.

[12] I. Paraschivoiu, F. Delclaux, Double Multiple Streamtube Model with Recent Improvements, Journal of Energy. 7 3 (1983) 250-255.

[13] H. Aagaard Madsen, U. Schmidt Paulsen, L. Vita, Analysis of VAWT aerodynamics and design using the Actuator Cylinder flow model, Proceedings of Torque 2012, The science of making torque from wind, Oldenburg, Germany, October 9-11, 2012.

[14] C.J. Simão Ferreira, The near wake of the VAWT: 2D and 3D views of the VAWT aerodynamics, PhD Thesis, Technische Universiteit Delft, The Netherlands, 2009.

[15] M. Raciti Castelli, A. Englaro, E. Benini, The Darrieus wind turbine: Proposal for a new performance prediction model based on CFD, Energy. 36 8 (2011) 4919-4934.

[16] A.A. Allet, S.S. Hallé, I. Paraschivoiu, Numerical Simulation of Dynamic Stall Around an Airfoil in Darrieus Motion, Journal of Solar Energy Engineering. 121 1 (1999) 69-76.

[17] C.J. Simão Ferreira, G. van Kuik, G. van Bussel, 2D CFD simulation of dynamic stall on a vertical axis wind turbine: verification and validation with PIV measurements, Proc. Of the 45th AIAA Aerospace Sciences Meeting 2007, 8-11 January 2007, Reno, NV, (Collection of Technical Papers - 45th AIAA Aerospace Sciences Meeting, 23 (2007) 16191-16201).

[18] L. Ferrari, A. Bianchini, Critical aspects in the design of a small-size Darrieus wind turbine, Proc. World Renewable Energy Congress (WREC) XI, Abu Dhabi, UAE, 25-30 September 2010.

[19] A. Bianchini, L. Ferrari, S. Magnani, Energy-yield-based optimization of an H-Darrieus wind turbine, Proceedings of the ASME Turbo Expo 2012, Copenhagen, Denmark, June 11-15, 2012.

[20] A. Rossetti, G. Pavesi, Comparison of different numerical approaches to the study of the H-Darrieus turbines start-up, Renewable Energy. 50 (2013) 7-19.

[21] R. Howell, N. Qin, J. Edwards, N. Durrani, Wind tunnel and numerical study of a small vertical axis wind turbine, Renewable Energy. 35 (2010) 412–422.

[22] T. Maître, E. Amet, C. Pellone, Modeling of the flow in a Darrieus water turbine: Wall grid refinement analysis and comparison with experiments, Renewable Energy. 51 (2013) 497-512.

[23] M. Raciti Castelli, G. Ardizzon, L. Battisti, E. Benini, G. Pavesi, Modeling strategy and numerical validation for Darrieus vertical axis micro-wind turbine, Proceedings of the ASME IMECE 2010, Vancouver, Canada, November 12-18, 2010.

[24] F. Trivellato, M. Raciti Castelli, On the Courant-Friedrichs-Lewy criterion of rotating grids in 2D vertical-axis wind turbine analysis, Renewable Energy. 62 (2014) 53-62.

[25] B. Yang, C. Lawn, Fluid dynamic performance of a vertical axis turbine for tidal currents, Renewable Energy. 36 (2011) 3355-3366.

[26] C.J. Simao Ferreira, H. Bijl, G. van Bussel, G. van Kuik, Simulating dynamic stall in a two-dimensional vertical-axis wind turbine: verification and validation with particle image velocimetry data, Wind Energy. 13(1) (2010) 1-17.

[27] H. Beri, Y. Yao, Effect of Camber Airfoil on Self Starting of Vertical Axis Wind Turbine, Journal of Environmental Science and Technology. 4 3 (2011) 302-312.

[28] S. Lain, C. Osorio, Simulation and evaluation of a straight-bladed Darrieus-type cross flow marine turbine, Journal of Scientific & Industrial Research. 69 (2010) 906-912.

[29] M.H. Mohamed, Performance investigation of H-rotor Darrieus turbine with new airfoil shapes, Energy. 47 (2012) 522-530.

[30] A. Untaroiu, H. G. Wood, P. E. Allaire, R. J. Ribando, Investigation of Self-Starting Capability of Vertical Axis Wind Turbines Using a Computational Fluid Dynamics Approach, Journal of Solar Energy Engineering. 133 4 (2011) 041010.

[31] P. Chatterjee, R. N. Laoulache, Performance Modeling of Ducted Vertical Axis Turbine Using Computational Fluid Dynamics, Marine Technology Society Journal. 47 4 (2013) 36-44.

[32] T. Ikoma, K. Masuda, S. Fujio, H. Nakada, H. Maeda, Characteristics of Hydrodynamic Forces and Torque on Darrieus Type Water Turbines for Current Power Generation Systems with CFD Computations, Proceedings of OCEANS, Kobe, Japan, April 8-11, 2008.

[33] M. Raciti Castelli, A. Dal Monte, M. Quaresimin, E. Benini, Numerical evaluation of aerodynamic and inertial contributions to Darrieus wind turbine blade deformation, Renewable Energy. 51 (2012) 101-112.

[34] C. Jian, J. Kumbernuss, H. X. Yang, X.Y.Wang, Influences of helix blade and unsymmetrical airfoil on theperformance of the Darrieus wind rotor, Proceedings of the International Conference on Applied Energy, Perugia, Italy, May 16-18, 2011.

[35] R. Gupta, A. Biswas, Computational fluid dynamics analysis of a twisted three-bladed H-Darrieus rotor, Journal of Renewable and Sustainable Energy. 2 4 (2010) 043111-043126.

[36] R. Gupta, S. Roy, A. Biswas, Computational fluid dynamics analysis of a twisted airfoil shaped two-bladed H-Darrieus rotor made from fibreglass reinforced plastic (FRP), International Journal of Energy and Environment, 1 6 (2010) 953-968.

[37] C. Kaminsky, A. Filush, P. Kasprzak, W. Mokhtar, A CFD Study of Wind Turbine Aerodynamics, Proceedings of the 2012 ASEE North Central Section Conference, Ohio Northern University, March 24, 2012.

[38] G. Colley, R. Mishra, H.V. Rao, R. Woolhead, Computational flow field analysis of a Vertical Axis Wind Turbine, Proceedings of the International Conference on Renewable Energies and Power Quality, Las Palmas de Gran Canaria, Spain, April 13-15, 2011.

[39] P. Sabaeifard, H. Razzaghi, A. Forouzandeh, Determination of Vertical Axis Wind Turbines Optimal Configuration through CFD Simulations, Proceedings of the International Conference on Future Environment and Energy, Singapore, 2012.

[40] A. Bianchini, L. Ferrari, S. Magnani, On the effects of a skewed flow on the performance of a three-bladed H-Darrieus turbine: experimental and theoretical analyses, Proceedings of the International Conference on Applied Energy (ICAE) 2012, Suzhou (China), July 5-8, 2012.

[41] F. Balduzzi, A. Bianchini, G. Ferrara, L. Ferrari, R. Maleci, Blade design criteria to compensate the flow curvature effects in H-Darrieus wind turbines, Journal of Turbomachinery. 137(1) (2015) 1-10.

[42] K. Cooper, Bluff-body blockage corrections in closed- an open-test-section wind tunnels, Wind Tunnel Wall Correction. Ewald BFR (ed.). AGARD-AG-336, RTO/NATO, Brussels (Belgium), 1998.

[43] L. Battisti, V. Dossena, G. Persico, L. Zanne, S. Dell'Anna, B. Paradiso, Aerodynamic Measurements on a Vertical Axis Wind Turbine in a Large Scale Wind Tunnel, J. Energy Resour. Technol.. 133(3) (2011) 031201-031201.

[44] P.G. Migliore, W.P. Wolfe, J.B. Fanucci, Flow Curvature Effects on Darrieus Turbine Blade Aerodynamics, Journal of Energy. 4(2) (1980) 49-55.

[45] Ansys, Inc., Fluent Theory Guide, release 14.5, 2013.

[46] D.C. Wilcox, Turbulence Modeling for CFD, DCW Industries Inc., La Canada (CA), 1998.

[47] F.R. Menter, M. Kuntz, R. Langtry, Ten Years of Industrial Experience with the SST Turbulence Model, Turbulence, Heat and Mass Transfer. 4 (2003) 625-632.

[48] F.R. Menter, Two-Equation Eddy-Viscosity Turbulence Models for Engineering Applications, AIAA Journal. 32 8 (1994) 1598-1605.

[49] J. Blazek, Computational Fluid Dynamics: Principles and Applications, Elsevier Science, Oxford (UK), 2001.

[50] H.K. Versteeg, W. Malalasekera, An introduction to computational fluid dynamics. The finite volume method, Longman, UK, 1995.

[51] J. Ferziger, M. Peric, Computational Methods for Fluid Dynamics, 3rd rev, Springer, Berlin, 2002.

[52] R. Peyret, Handbook of Computational Fluid Mechanics, Academic Press Inc., Oxford, 1996.

[53] R.S. Amano, B. Sunden, Computational Fluid Dynamics and Heat Transfer: Emerging Topics, WIT Press, Southampton, UK, 2011.

[54] C.J. Hearn, The Dynamics of Coastal Models, Cambridge University Press, Cambridge, UK, 2008.

[55] F. Balduzzi, A. Bianchini, F.A. Gigante, G. Ferrara, M.S. Campobasso, L. Ferrari, L., Parametric and Comparative Assessment of Navier-Stokes CFD Methodologies for Darrieus Wind Turbine Performance Analysis, Proceedings of the ASME Turbo Expo 2015, Montreal, Canada, June 15-19, 2015.

[56] P. Vittecoq, A. Laneville, The aerodynamic forces for a Darrieus rotor with straight blades: Wind tunnel measurements, Journal of Wind Engineering and Industrial Aerodynamics. 15(1-3) (1983) 381-388.

[57] I. Paraschivoiu, Predicted and Experimental Aerodynamic Forces on the Darrieus Rotor, Journal of Energy. 7(6) (1983) 610-615.

[58] A. Bianchini, L. Ferrari, E.A. Carnevale, A model to account for the Virtual Camber Effect in the Performance Prediction of an H-Darrieus VAWT Using the Momentum Models, Wind Engineering. 35(4) (2011) 465-482.

[59] A. Bianchini, L. Ferrari, S. Magnani, Start-up behavior of a three-bladed h-Darrieus VAWT: experimental and numerical analysis, Proceedings of the ASME Turbo Expo 2011, Vancouver, Canada, June 6-10, 2011.

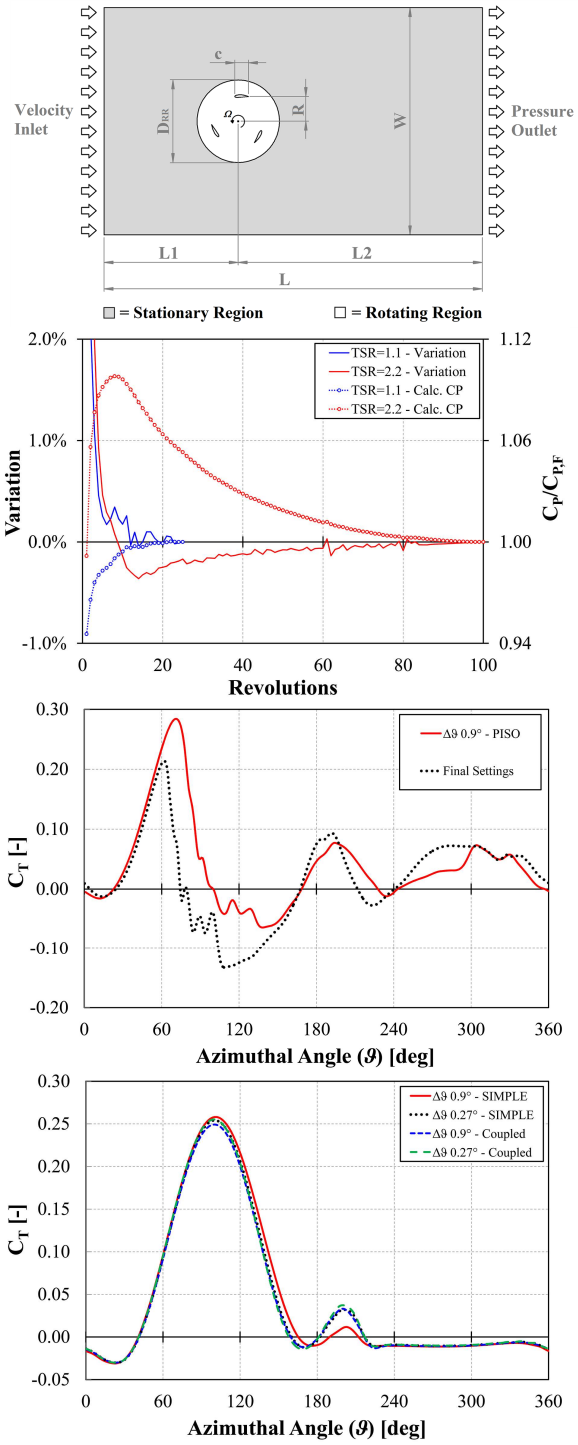
Velocity Inlet
Pressure Outlet
c
D_DR
R
W
L1
L2
L
= Stationary Region
= Rotating Region
TSR=1.1 - Variation
TSR=2.2 - Variation
TSR=1.1 - Calc. CP
TSR=2.2 - Calc. CP
Variation
C_P/C_P,F
Revolutions
Δϑ 0.9° - PISO
Final Settings
C_T [-]
Azimuthal Angle (ϑ) [deg]
Δϑ 0.9° - SIMPLE
Δϑ 0.27° - SIMPLE
Δϑ 0.9° - Coupled
Δϑ 0.27° - Coupled
C_T [-]
Azimuthal Angle (ϑ) [deg]

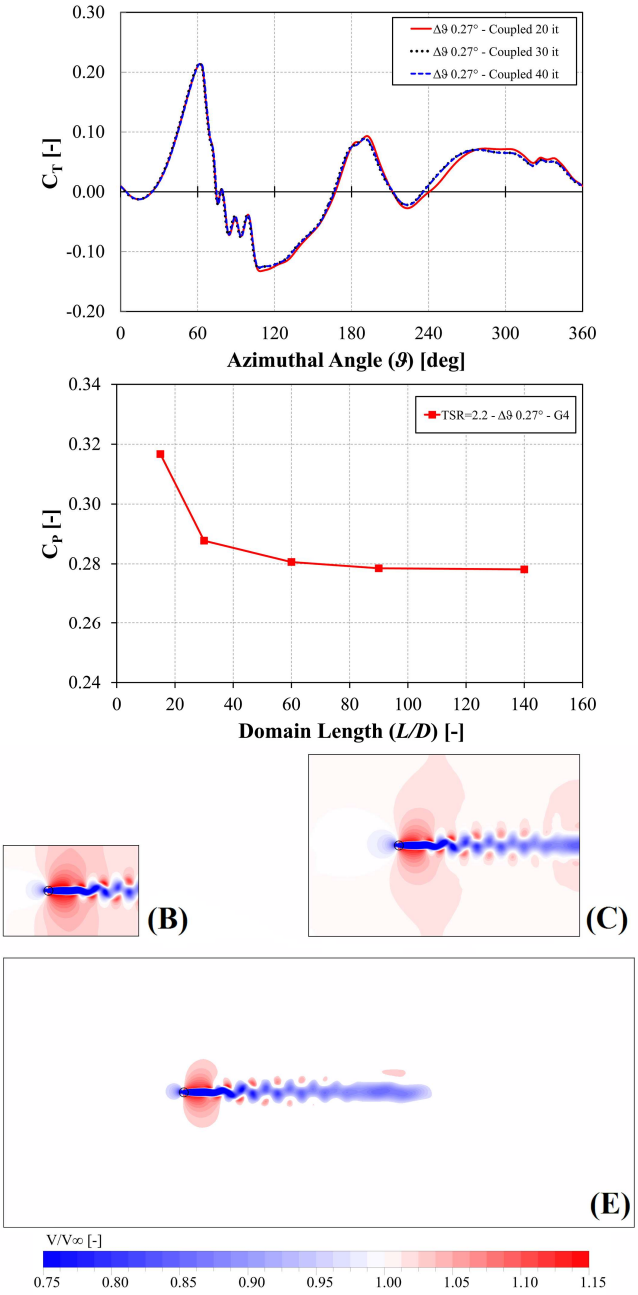
Δϑ 0.27° - Coupled 20 it
Δϑ 0.27° - Coupled 30 it
Δϑ 0.27° - Coupled 40 it
C_T [-]
Azimuthal Angle (ϑ) [deg]
TSR=2.2 - Δϑ 0.27° - G4
C_P [-]
Domain Length (L/D) [-]
(B)
(C)
(E)
V/V∞ [-]

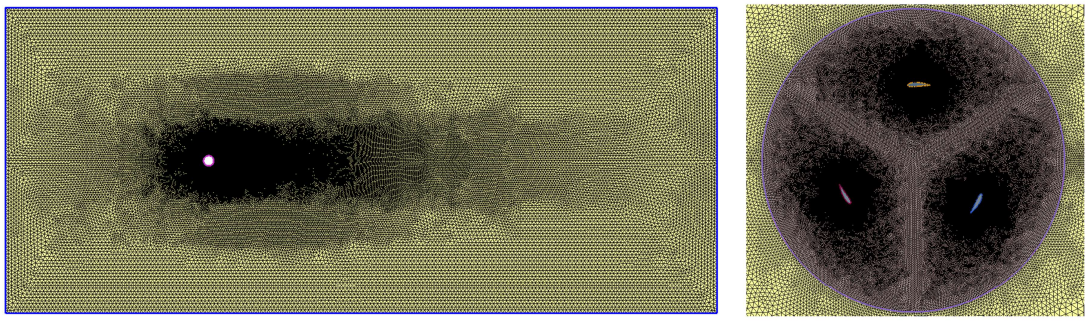

(a) (b)

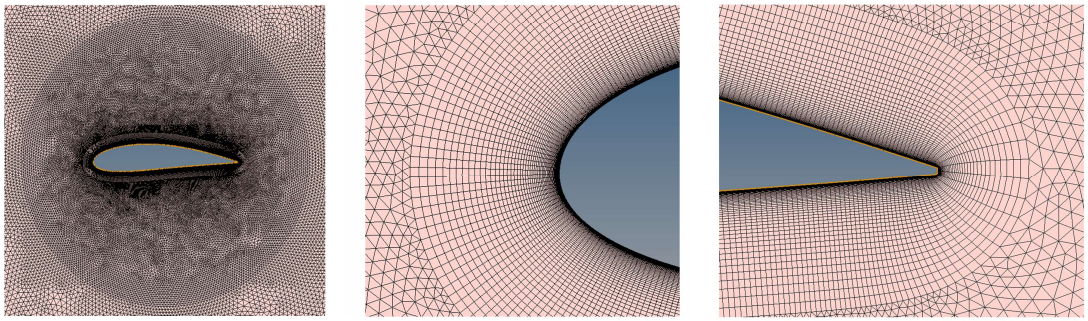

(c) (d) (e)

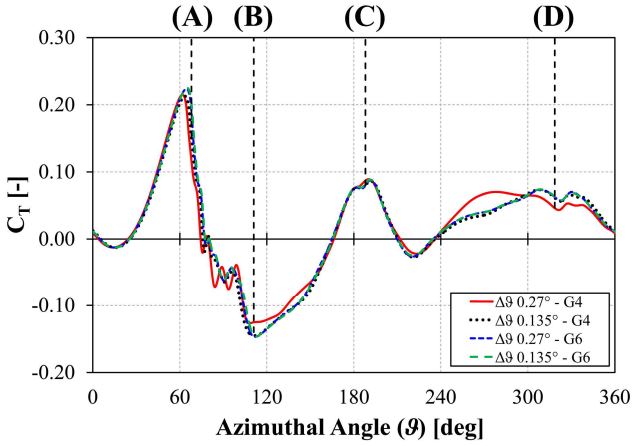
(A)
(B)
(C)
(D)
0.30
0.20
0.10
0.00
-0.10
-0.20
C_T [-]
0
60
120
180
240
300
360
Azimuthal Angle (ϑ) [deg]
Δϑ 0.27° - G4
Δϑ 0.135° - G4
Δϑ 0.27° - G6
Δϑ 0.135° - G6

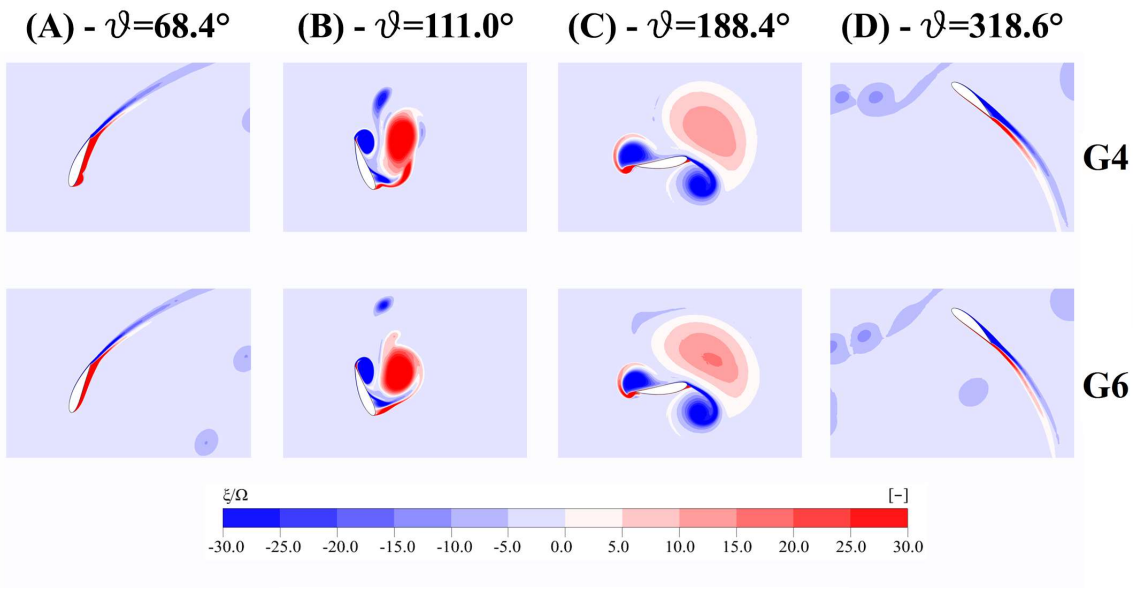
(A) - ϑ=68.4°
(B) - ϑ=111.0°
(C) - ϑ=188.4°
(D) - ϑ=318.6°
G4
G6
ξ/Ω
[-]
-30.0 -25.0 -20.0 -15.0 -10.0 -5.0 0.0 5.0 10.0 15.0 20.0 25.0 30.0

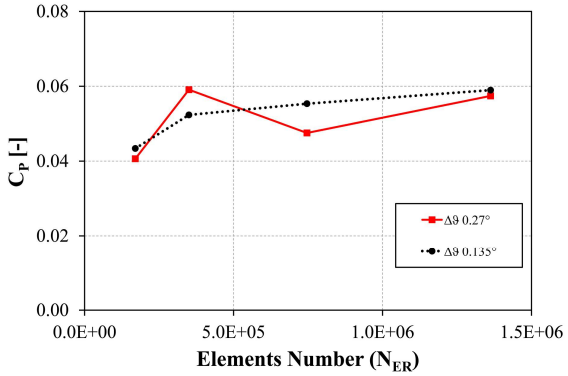
0.08
0.06
0.04
0.02
0.00
C_P [-]
Δϑ 0.27°
Δϑ 0.135°
0.0E+00
5.0E+05
1.0E+06
1.5E+06
Elements Number (N_ER)

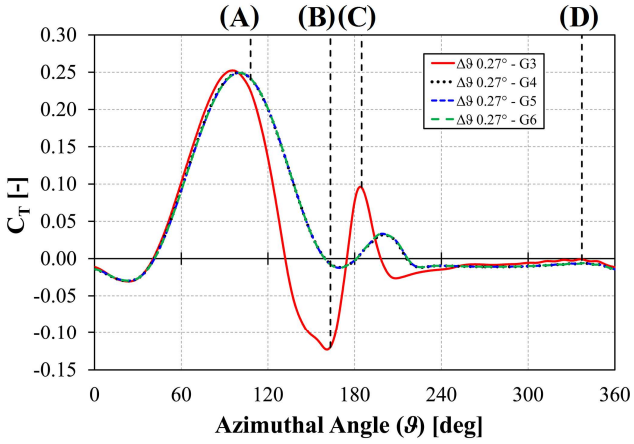
(A)
(B)(C)
(D)
0.30
0.25
0.20
0.15
0.10
0.05
0.00
-0.05
-0.10
-0.15
C_T [-]
Δϑ 0.27° - G3
Δϑ 0.27° - G4
Δϑ 0.27° - G5
Δϑ 0.27° - G6
0
60
120
180
240
300
360
Azimuthal Angle (ϑ) [deg]

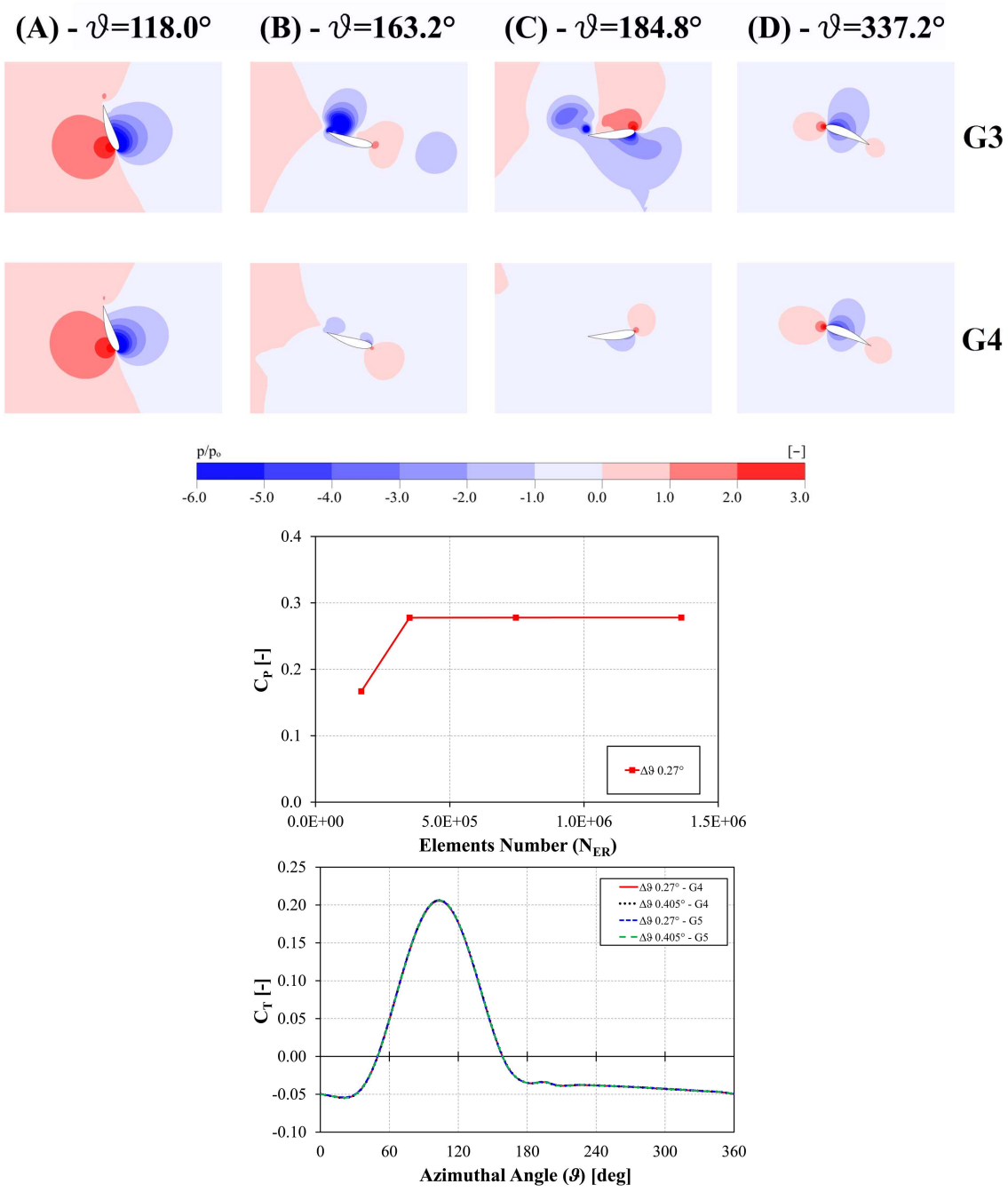
(A) - ϑ=118.0°
(B) - ϑ=163.2°
(C) - ϑ=184.8°
(D) - ϑ=337.2°
G3
G4
p/p∞
[-]
-6.0
-5.0
-4.0
-3.0
-2.0
-1.0
0.0
1.0
2.0
3.0
C_P [-]
0.4
0.3
0.2
0.1
0.0
0.0E+00
5.0E+05
1.0E+06
1.5E+06
Δϑ 0.27°
Elements Number (N_ER)
C_T [-]
0.25
0.20
0.15
0.10
0.05
0.00
-0.05
-0.10
0
60
120
180
240
300
360
Δϑ 0.27° - G4
Δϑ 0.405° - G4
Δϑ 0.27° - G5
Δϑ 0.405° - G5
Azimuthal Angle (ϑ) [deg]

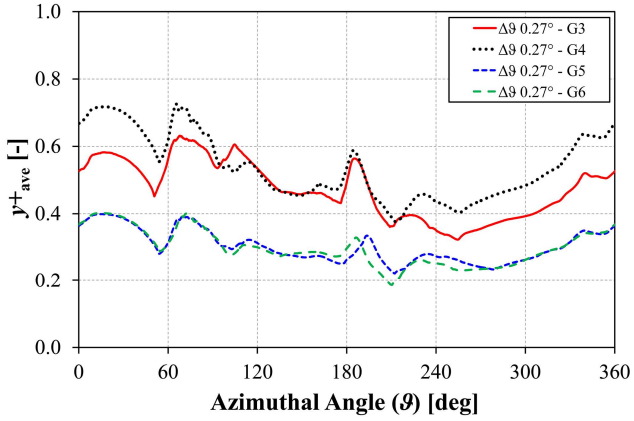
Δϑ 0.27° - G3
Δϑ 0.27° - G4
Δϑ 0.27° - G5
Δϑ 0.27° - G6
y+ave [-]
Azimuthal Angle (ϑ) [deg]

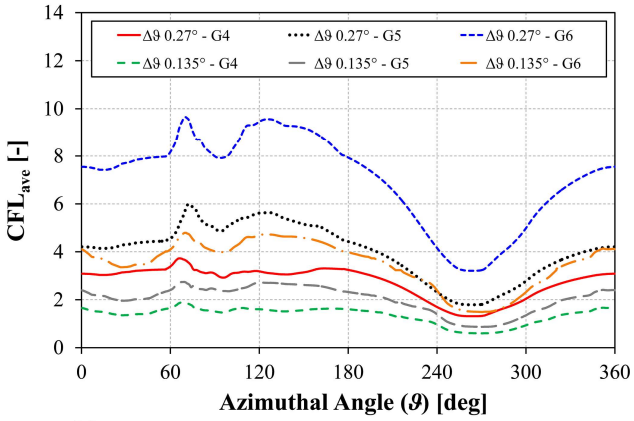
Δϑ 0.27° - G4
Δϑ 0.27° - G5
Δϑ 0.27° - G6
Δϑ 0.135° - G4
Δϑ 0.135° - G5
Δϑ 0.135° - G6
CFLave [-]
Azimuthal Angle (ϑ) [deg]

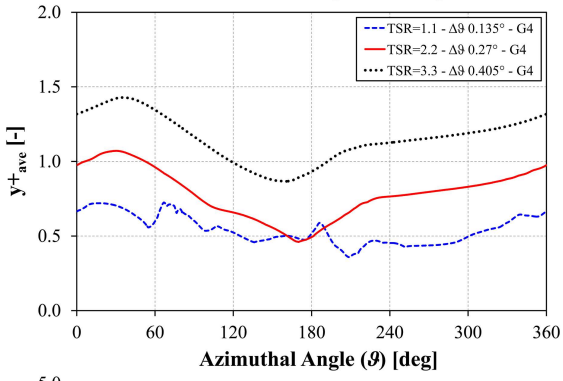
TSR=1.1 - Δϑ 0.135° - G4
TSR=2.2 - Δϑ 0.27° - G4
TSR=3.3 - Δϑ 0.405° - G4
y+ave [-]
Azimuthal Angle (ϑ) [deg]

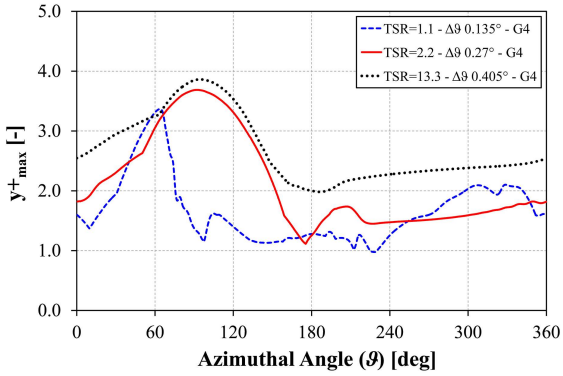
TSR=1.1 - Δϑ 0.135° - G4
TSR=2.2 - Δϑ 0.27° - G4
TSR=13.3 - Δϑ 0.405° - G4
y+max [-]
Azimuthal Angle (ϑ) [deg]

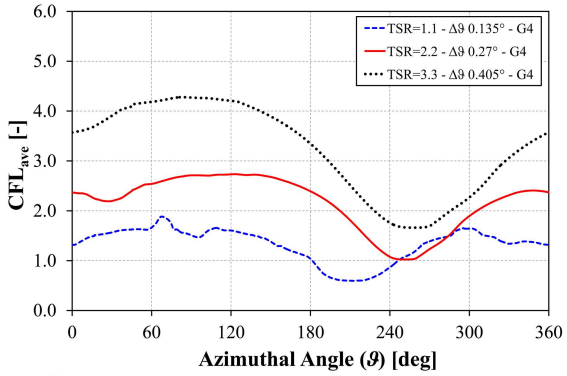
TSR=1.1 - Δϑ 0.135° - G4
TSR=2.2 - Δϑ 0.27° - G4
TSR=3.3 - Δϑ 0.405° - G4
CFL_ave [-]
Azimuthal Angle (ϑ) [deg]

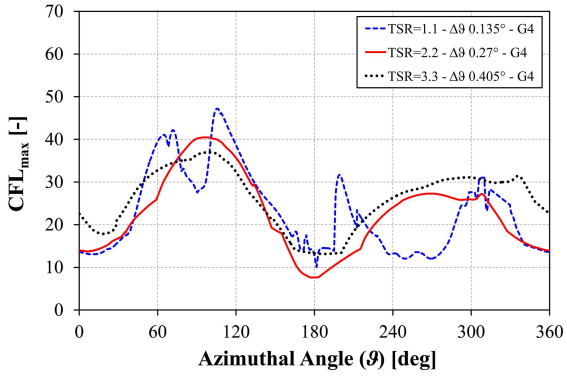
TSR=1.1 - Δϑ 0.135° - G4
TSR=2.2 - Δϑ 0.27° - G4
TSR=3.3 - Δϑ 0.405° - G4
CFL_max [-]
Azimuthal Angle (ϑ) [deg]

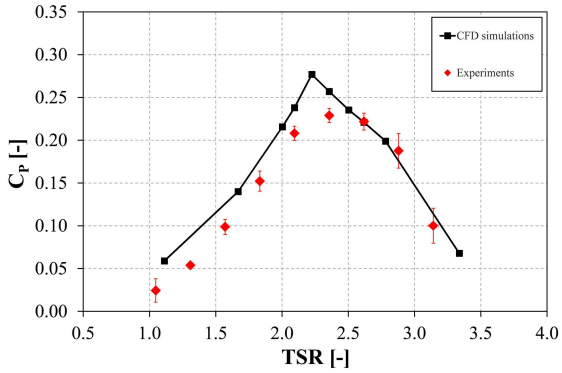
CFD simulations
Experiments
C_P [-]
TSR [-]

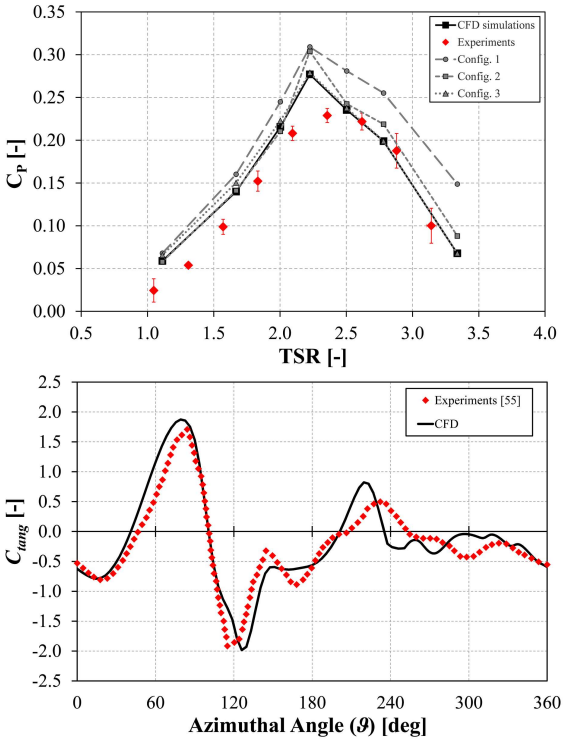
CFD simulations
Experiments
Config. 1
Config. 2
Config. 3
C_P [-]
TSR [-]
Experiments [55]
CFD
C_{tang} [-]
Azimuthal Angle (ϑ) [deg]